Chinese Chemical Letters 31 (2020) 3153–3157

Contents lists available at ScienceDirect

Chinese Chemical Letters

journal homepage: www.elsevier.com/locate/cclet

Communication

A self-assembling peptide targeting VEGF receptors to inhibit angiogenesis

Shifang Wen[a,b,1], Kuo Zhang[b,1], Yuan Li[b], Jiaqi Fan[b], Ziming Chen[a,b], Jingping Zhang[a,*], Hao Wang[b], Lei Wang[b,*]

[a] Faculty of Chemistry, Northeast Normal University, Changchun 130024, China
[b] Laboratory for Biomedical Effects of Nanomaterials and Nanosafety, National Center for Nanoscience and Technology (NCNST), Beijing 100190, China

ARTICLE INFO

Article history:
Received 28 February 2020
Received in revised form 30 March 2020
Accepted 30 March 2020
Available online 23 April 2020

Keywords:
Self-assembly
Peptide
VEGF
Angiogenesis
Biomimetic

ABSTRACT

Vascular endothelial growth factor (VEGF)-vascular endothelial growth factor receptor (VEGFR) pathways are essential in tumor angiogenesis, growth and metastasis. Studies on anti-angiogenic therapy have been mostly focused on the blockage of VEGF-VEGFR pathways. We report an extracellularly transformable peptide-based nanomaterial to develop artificial extracellular matrix (ECM)-like networks for high-efficient blockage of natural VEGF-VEGFR interactions. The transformable peptide-based nanomaterial transforms from nanoparticles into nanofibers upon binding to VEGFR in solution. In addition, the transformable peptide-based nanomaterial forms ECM-like fibrous networks on VEGFR overexpressed cells, inhibiting the VEGF-VEGFR interactions and the subsequent angiogenesis. The tube formation is reduced by nearly 85.1% after treatment. This strategy shows excellent potential for anti-angiogenesis, and inhibition of tumor invasion and metastasis.

Angiogenesis has been recognized as a target for the tumor therapy [1]. First, anti-angiogenic therapy reduces the supply of oxygen and nutrition for tumors, leading to the inhibition of tumor progression. Second, the inhibition of angiogenesis reduces the possibility of metastasis of tumor cells from the blood circulation. Third, the endothelial cells that are the basic component of angiogenesis, are considered genetically stable. Therefore, the anti-angiogenic therapy is drug-resistance free strategy [2]. Thus far, anti-angiogenesis has been regarded as a combined clinical strategy with other treatments for cancer [3,4]. The anti-angiogenic therapies have shown the high-efficiency [5].

Unlike normal blood vessels, tumor vessels are structurally and functionally abnormal [6,7]. These characteristics of solid tumors are the major factor in the failure of conventional chemotherapy to achieve expected effectiveness [8]. Vascular endothelial growth factor (VEGF)-vascular endothelial growth factor receptor (VEGFR) pathways have the prominent roles in tumor angiogenesis, growth and metastasis. The VEGF family exerts their biological functions through the interaction with tyrosine kinase receptors, VEGFR [9,10]. Binding of VEGF to VEGFR leads to proliferation, migration, invasion of endothelial cell and high vascular permeability through downstream signaling pathways. Therapeutic angiogenesis studies based on anti-VEGFR antibodies and tyrosine kinase inhibitors have been mostly focused on the disruption of VEGF-VEGFR pathways [11].

Peptide has been paid much attention due to its biological activity, biocompatibility and so on [12]. Many peptides have been developed to inhibit protein-protein interactions [13–15]. Rationally designed peptides can mimic the binding regions in protein-protein and antagonize a biological activity of target protein with high specificity. In recent years, many researchers have designed many antagonist peptides through a rational approach [16–19]. In our group, we developed a process-biomimetic strategy to develop artificial extracellular matrix (ECM)-like networks for blockage of natural protein-protein interactions [20]. The strategy could be utilized for the blockage of VEGF and VEGFR interactions for the inhibition of angiogenesis.

In the present study, we designed a kind of self-assembling peptide, bispyrene-KLVFF-PCAIWF, which can bind to VEGFR and decrease the activation of the downstream pathway for inhibiting the migration of endothelial cells and the resulting angiogenesis (Scheme 1). The bispyrene-KLVFF-PCAIWF peptide for binding VEGFR (BV) was designed with three modules: First, the hydrophobic bispyrene (BP) with aggregation-induced emission

* Corresponding authors.
E-mail addresses: zhangjp162@nenu.edu.cn (J. Zhang), wanglei@nanoctr.cn (L. Wang).
[1] These authors contributed equally to this work.

https://doi.org/10.1016/j.cclet.2020.03.077

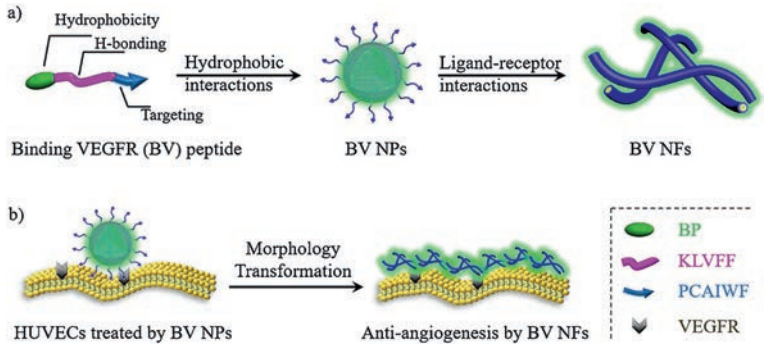

Scheme 1. The schematic illustration for the transformation of binding VEGFR (BV) peptide upon VEGFR (a) and on HUVECs for anti-angiogenesis (b).

(AIE) characteristics for the formation of nanoaggregates and the fluorescence imaging [21]; second, the KLVFF peptide scaffold for the formation of fibers with β-sheet structures; and the last, the PCAIWF peptide motif as a ligand to bind to VEGFR and subsequently induce structural transformation [22]. The BV peptide first self-assembled into nanoparticles (NPs) and then transformed into nanofibers (NFs), On the one hand, the structural transformation from BV NPs into BV NFs induced by VEGFR was validated *in vitro* by multiple techniques. On the other hand, the VEGFR was bound by the ECM-like nanofibrous networks for highly efficient inhibition of the migration of human umbilical vein endothelial cells (HUVECs) and the resulting angiogenesis. In addition, The BV peptide showed higher efficient inhibition the migration of endothelial cells compared with the BP-KAAGG-PCAIWF (C-BV) peptide as a control with the mutation of assembling peptide KLVFF. The BV NPs showed excellent potential as an effective VEGFR antibody, which *in situ* transformed into capturing networks extracellularly for the inhibition of tumor invasion and metastasis.

The BV peptide BP-FFVLK-PCAIWF and C-BV peptide BP-GGAAK-PCAIWF (Fig. 1a) were prepared based on the Fmoc mode of solid-phase peptide synthesis techniques. The matrix-assisted laser desorption/ionization time-of-flight (MALDI-TOF) mass spectra were recorded to determine molecular structures of BV and C-BV peptides (Figs. S1 and S2 in Supporting information). The BV NPs were prepared by the rapid precipitation method *via* injecting the dimethyl sulfoxide (DMSO) solution of BV peptide (4 mmol/L, 5 μL) into water (995 μL). UV-vis and fluorescence spectra were utilized to monitor the process that BV peptide self-assembled into BV NPs. The intensity of absorption peaks of BV monomers at around 300–400 nm decreased and the bathochromic absorption peak increased with ratio of water to DMSO increasing, indicating the formation of BV NPs (Fig. 1b) [21]. In addition, a fluorescence increase with the maximum at 520 nm was observed, probably due to the formation of BP aggregates (Fig. 1c) [23,24]. The circular dichroism (CD) (Fig. 1d) and the fourier transform infrared spectroscopy (FT-IR) (Fig. 1e) measurements clearly demonstrated that the BV peptide in NPs showed random coil secondary structure. Therefore, the self-assembly of BV peptide into BV NPs by rapid precipitation method was probably driven by hydrophobicity of BP, not the hydrogen-bonds of the KLVFF sequence. The C-BV peptide showed similar aggregation behavior to the BV peptide (Figs. S3 and S4 in Supporting information).

The BV NPs may transform into BV NFs by interacting with VEGFR due to the specific interactions between PCAIWF in BV NPs and VEGFR. In order to study the morphology change of BV NPs, we added VEGFR protein to the solutions of BV NPs and C-BV NPs, respectively. The morphological change in BV NPs was determined by TEM over 72 h. The results confirmed that interactions between

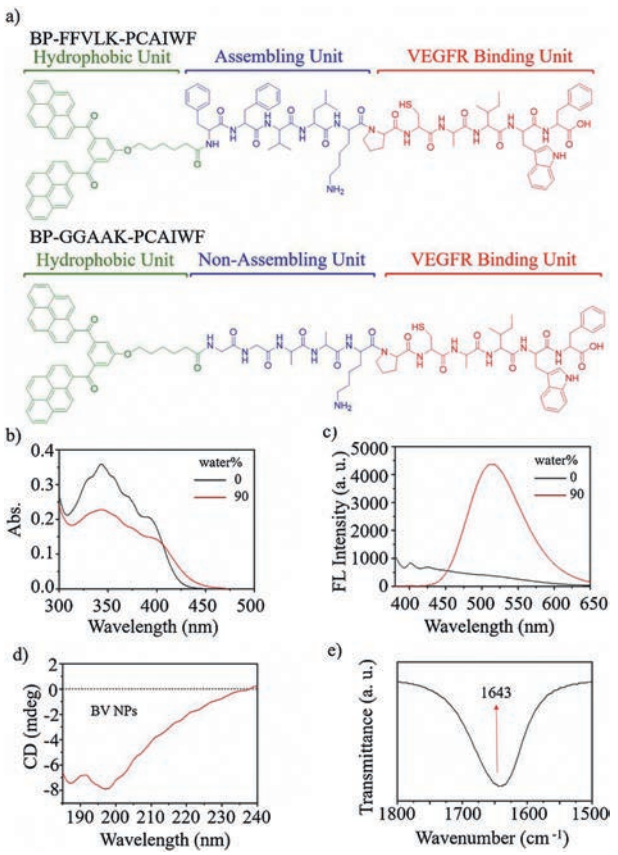

Fig. 1. Molecular design and self-assembly of binding VEGF (BV) peptides. (a) Molecular structure of BV peptide and C-BV peptide. (b) UV-vis and (c) fluorescence spectra characteristics of self-assembly process to form BV NPs ($c = 2.0 \times 10^{-5}$ mol/L) in mixed H_2O/DMSO solutions. (d) CD spectral characterization of BV NPs at 0 h. (e) FT-IR spectrum of BV NPs at 0 h.

VEGFR and PCAIWF were necessary for the process of morphological transformation from BV NPs into BV NFs (Fig. 2a). Furthermore, C-BV NPs did not transform morphologies through the interaction between PCAIWF and VEGFR during this period (Fig. 2b), showing that the hydrogen-bond unit, KLVFF, was essential for the transformation from BV NPs to BV NFs.

The CD experiments were performed to verify the conformation and secondary structure of BV NFs. The BV NPs incubated with VEGFR formed an obvious hydrogen-bonding β-sheet structure after 72 h, owing to a negative CD signal at 230 nm and a positive one at 200 nm (Fig. 2c) [25]. The C-BV NPs with VEGFR and the BV NPs without VEGFR showed no obvious secondary structure during

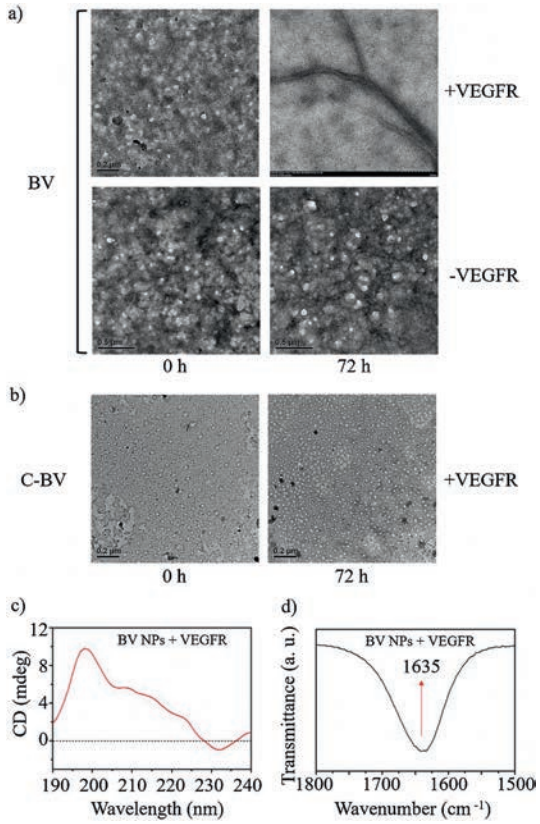

Fig. 2. Structural transformation of BV peptide from nanoparticles into nanofibers. (a) TEM images of BV NPs structural evolution in the absence/presence of VEGFR in mixed H_2O/DMSO solutions ($c = 2.0 \times 10^{-5}$ mol/L). Scale bar: 0.2 μm (upper), 0.5 μm (lower). (b) TEM images of C-BV NPs in the presence of VEGFR in mixed H_2O/DMSO solutions ($c = 2.0 \times 10^{-5}$ mol/L). Scale bar: 0.2 μm. (c) CD spectral characterization with the β-sheet structure formation of BV NPs with VEGFR at 72 h. (d) FT-IR spectrum of BV NPs with VEGFR at 72 h.

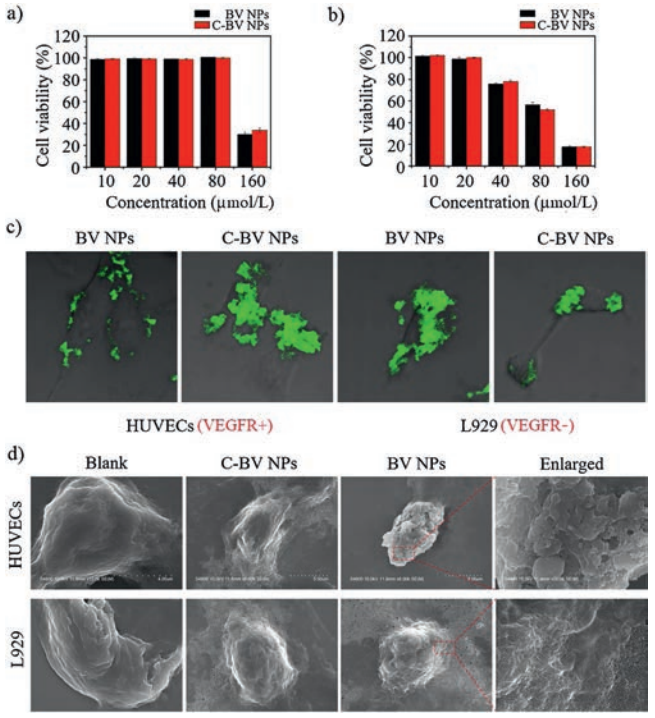

Fig. 3. Biosafety in vitro, characterization of transformation from nanoparticles into nanofibers on cell surfaces induced by VEGFR. Cell cytotoxicity assay of BV NPs or C-BV NPs with (a) HUVEC cells or (b) L929 cells for 72 h. (c) CLSM images of HUVEC cells and L929 cells incubated with BV NPs (20 μmol/L) and C-BV NPs (20 μmol/L) for 4 h. (d) SEM images of cell surfaces of HUVECs or L929 treated with BV NPs or C-BV NPs, and untreated cells as blank groups.

this period (Fig. S5 in Supporting information). The detailed packing structure of BV in BV NFs was also studied by FT-IR. The characteristic C = O stretching vibration at 1635 cm^{-1} indicated the parallel β-sheet structure (Fig. 2d) [26]. All the results above suggested that BV NPs transformed morphologies through the interaction between PCAIWF and VEGFR, and the KLVFF was also crucial for the transformation with β-sheet structure formation through hydrogen-bonds in BV NFs.

In order to study the VEGFR-induced morphological transformation on cell surfaces, BV NPs and C-BV NPs were tested with HUVECs with highly expressed VEGFR and L929 as a control cell line. The cell viability of HUVECs and L929 cells were firstly measured when incubated with BV NPs and C-BV NPs, respectively. As shown in Figs. 3a and b, the BV NPs and C-BV NPs showed cytotoxicity to HUVECs and L929 cells at high concentrations, but almost no toxic below 20 μmol/L. For the following cellular experiment, the concentration of BV NPs and C-BV NPs were chosen as 20 μmol/L to confirm that the biological effects were no related with cell killing. First, BV NPs and C-BV NPs (20 μmol/L) were incubated with HUVECs and L929 for 4 h, respectively. The resultant samples were utilized for confocal laser scanning microscopy (CLSM) measurements. As shown in Fig. 3c, green fluorescence was observed on the surface of BV NPs-treated HUVECs, which was originated from aggregated BP. These results implied that BV NPs may bind to VEGFR on cells and transform into BV NFs, attaching to the cell surfaces. C-BV NPs-treated HUVECs showed green fluorescence inside the cells, indicating that the C-BV NPs were mainly taken up by the cells as usual. Moreover, for BV NPs- or C-BV NPs-treated L929 cells, green fluorescence was mainly observed intracellularly, indicating the internalized BV NPs or C-BV NPs. These cellular experimental results indicated that the BV NPs could transform into BV NFs on HUVECs through binding overexpressed VEGFR.

To further validate the specific binding between BV NPs and VEGFR and the corresponding transformation, scanning electron microscopy (SEM) was utilized for characterize the BV NPs and C-BV NPs incubated with HUVECs and L929 cells, respectively. BV NPs or C-BV NPs were incubated with HUVEC or L929 for 4 h, followed by gradient dehydration for SEM measurements. As shown in Fig. 3d, The BV NPs-treated HUVECs showed fibrous networks on cell surfaces. However, BV NPs-treated L929 cells, C-BV NPs treated L929 cells or HUVECs showed similar morphology with corresponding blank cells.

To verify inhibition of angiogenesis, the tube formation and the wound healing experiments of HUVECs were performed using BV NPs and C-BV NPs at the concentration of 20 μmol/L. The wound healing rate of HUVECs was defined to 24.8% by BV NPs treatment at 48 h after scratching, which was much lower than 80.3% of blank group and 72.6% C-BV NPs-treated group (Figs. 4a and b). These results confirmed that BV NPs significantly inhibited the horizontal migration of HUVECs through binding with VEGFR, which was more efficacious than that of C-BV NPs. On the other hand, there was no obvious difference among the three groups of L929 cells, which suggested that both BV NPs and C-BV NPs were only effective on cells with highly expressed VEGFR. BV NPs and C-BV NPs may bind to VEGFR and prevent VEGF-VEGFR signaling pathway, resulting in the anti-angiogenesis. The tube formation assay was utilized to investigate how BV NPs interfered with the process of tube formation. The results showed that BV NPs could inhibit tube formation with high-efficiency, which was higher than that

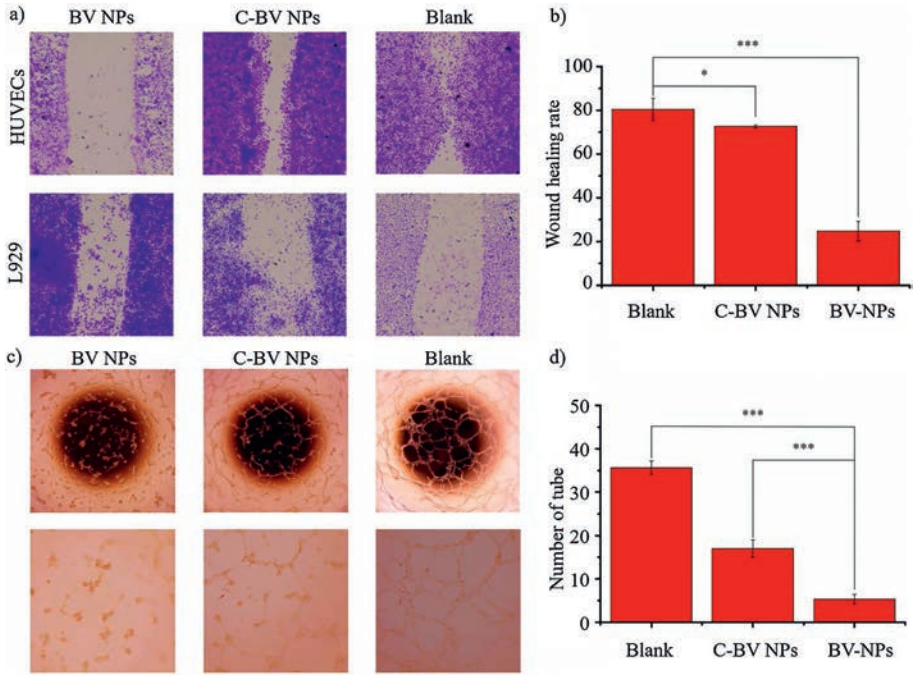

Fig. 4. Peptides bind to VEGFR and inhibit the migration and vessel formation of HUVECs. Microscopic images of wound healing (a) and tube formation (c), and quantitative analysis (b and d). The data are analyzed by a Student's t-test. Statistical significance is indicated as $^{*}P < 0.05$, $^{**}P < 0.01$, $^{***}P < 0.001$.

of C-BV NPs (Figs. 4c and d). BV NPs and C-BV NPs could inhibit the migration and tube formation *via* binding to VEGFR. The BV NPs showed much higher efficiency than C-BV NPs. These results implied the importance of transformation of BV NPs on cell surfaces, enabling the high-efficient binding. C-BV NPs were mainly taken up by cells and could not show highly efficient inhibition of binding to the extracellular domain of VEGFR.

In summary, the vascular endothelial growth factor receptors are essential in the process of angiogenesis, the inhibitors of which play an important role in the clinic. In this study, a self-assembling peptide (BV) with transformable capability was demonstrated to inhibit VEGF-VEGFR interactions specifically. BV self-assembled into BV NPs and transformed *in situ* into BV NFs, which was confirmed by multiple techniques in solution and *in vitro*. Therefore, BV NPs inhibited the migration of HUVECs *in vitro* and inhibited angiogenesis *in vivo*. Collectively, our results suggested that BV peptide was an effective VEGFR antibody for anti-angiogenesis therapy.

The transformable self-assembling peptide was a kind of nanomaterials, which was widely applied for biomedical applications with many advantages, such as long-circulation, high stability, and so on [27,28]. Meanwhile, the transformable self-assembling peptide was a smart nanomaterial, transforming the morphologies during applied *in vivo* [29]· The transformation from NPs into NFs through ligand-receptor interactions of BV peptide was initially inspired by the ECM formation process, which involves globular fibronectin transform into fibrous fibronectin process to form fibrous networks [26]. Therefore, this kind of transformable self-assembling peptide was a kind of process-biomimetic strategy, developing ECM-like networks as peptide antibody networks to block extracellular protein-protein interactions. The peptide antibody was formed on cell surfaces as ECM-like fibrous networks, which showed high efficiency and high stability with multivalent effect. The ECM-like peptide antibody showed great potential in clinical applications.

Declaration of competing interest

The authors declare that they have no known competing financial interests or personal relationships that could have appeared to influence the work reported in this paper.

Acknowledgments

This work was supported by the National Natural Science Foundation of China (Nos. 51890891, 51725302, 21807020, 51573031 and 51573032), National Key R&D Program of China (No. 2018YFE0205400), Science Fund for Creative Research Groups of the National Natural Science Foundation of China (No. 11621505) and CAS Interdisciplinary Innovation Team.

Appendix A. Supplementary data

Supplementary material related to this article can be found, in the online version, at doi:https://doi.org/10.1016/j.cclet.2020.03.077.

References

[1] J. Folkman, M. Bach, J.W. Rowe, et al., N. Engl. J. Med. 285 (1971) 1182–1186.
[2] J. Folkman, Nat. Rev. Drug. Discov. 6 (2007) 273–286.
[3] D.M. Chase, D.J. Chaplin, B.J. Monk, Gynecol. Oncol. 145 (2017) 393–406.
[4] N. Ferrara, A.P. Adamis, Nat. Rev. Drug. Discov. 15 (2016) 385–403.
[5] A.R. Reynolds, I.R. Hart, A.R. Watson, et al., Nat. Med. 15 (2009) 392–400.
[6] A.S. Chung, N. Ferrara, Annu. Rev. Cell Dev. Biol. 27 (2011) 563–584.
[7] A.S. Chung, J. Lee, N. Ferrara, Nat. Rev. Cancer 10 (2010) 505–514.
[8] D. Fukumura, J. Kloepper, Z. Amoozgar, et al., Nat. Rev. Clin. Oncol. 15 (2018) 325–340.
[9] R.S. Apte, D.S. Chen, N. Ferrara, Cell 176 (2019) 1248–1264.
[10] R.K. Jain, Cancer Cell 26 (2014) 605–622.
[11] V.L. Heath, R. Bicknell, Nat. Rev. Clin. Oncol. 6 (2009) 395–404.
[12] K. Zhang, Y.J. Gao, P.P. Yang, et al., Adv. Healthc. Mater. 7 (2018) 1800344.
[13] R.J. Giordanoa, M. Cardó-Vilaa, A. Salameha, et al., PNAS 11 (2010) 5112–5117.
[14] H. Koide, K. Yoshimatsu, Y. Hoshino, et al., Nat. Chem. 9 (2017) 715–722.
[15] B. Yu, D. Hwang, H. Jeon, Angew. Chem. Int. Ed. 58 (2018) 2005–2010.
[16] G.B. Qi, Y.J. Gao, L. Wang, H. Wang, Adv. Mater. 30 (2018) 1703444.

[17] Q. Luo, Y.X. Lin, P.P. Yang, et al., Nat. Commun. 9 (2018) 1802.
[18] P.P. Yang, C. Yang, K. Zhang, L. Wang, H. Wang, Chin. Chem. Lett. 29 (2018) 1811–1814.
[19] P.P. He, X.D. Li, L. Wang, H. Wang, Acc. Chem. Res. 52 (2019) 367–378.
[20] X.X. Hu, P.P. He, G.B. Qi, et al., ACS Nano 11 (2017) 4086–4096.
[21] L. Wang, W. Li, J. Lu, et al., J. Phys. Chem. C 117 (2013) 26811–26820.
[22] J.S. Michaloski, A.R. Redondo, L.S. Magalhães, Sci. Adv. 2 (2016) e1600611.
[23] A.P. Xu, P.P. Yang, C. Yang, et al., Nanoscale 8 (2016) 14078–14083.
[24] E.T. Kaiser, H. Wang, V. Stepanenko, et al., Angew. Chem. Int. Ed. 46 (2007) 5541–5544.
[25] V. Castelletto, I.W. Hamley, P.J.F. Harris, et al., J. Phys. Chem. B 113 (2009) 9978–9987.
[26] L. Niu, L. Liu, M. Xu, et al., Chem. Commun. 50 (2014) 8923–8926.
[27] J.X. Ding, X.R. Feng, Z.Y. Jiang, et al., Biomacromolecules 20 (2019) 4258–4271.
[28] J.X. Ding, J.J. Chen, L.Q. Gao, et al., Nano Today 29 (2019) 100800.
[29] K. Zhang, P.P. Yang, J.P. Zhang, L. Wang, H. Wang, Chin. Chem. Lett. 28 (2017) 1808–1816.